iScience

CellPress
OPEN ACCESS

Article

Network model integrated with multi-omic data predicts MBNL1 signals that drive myofibroblast activation

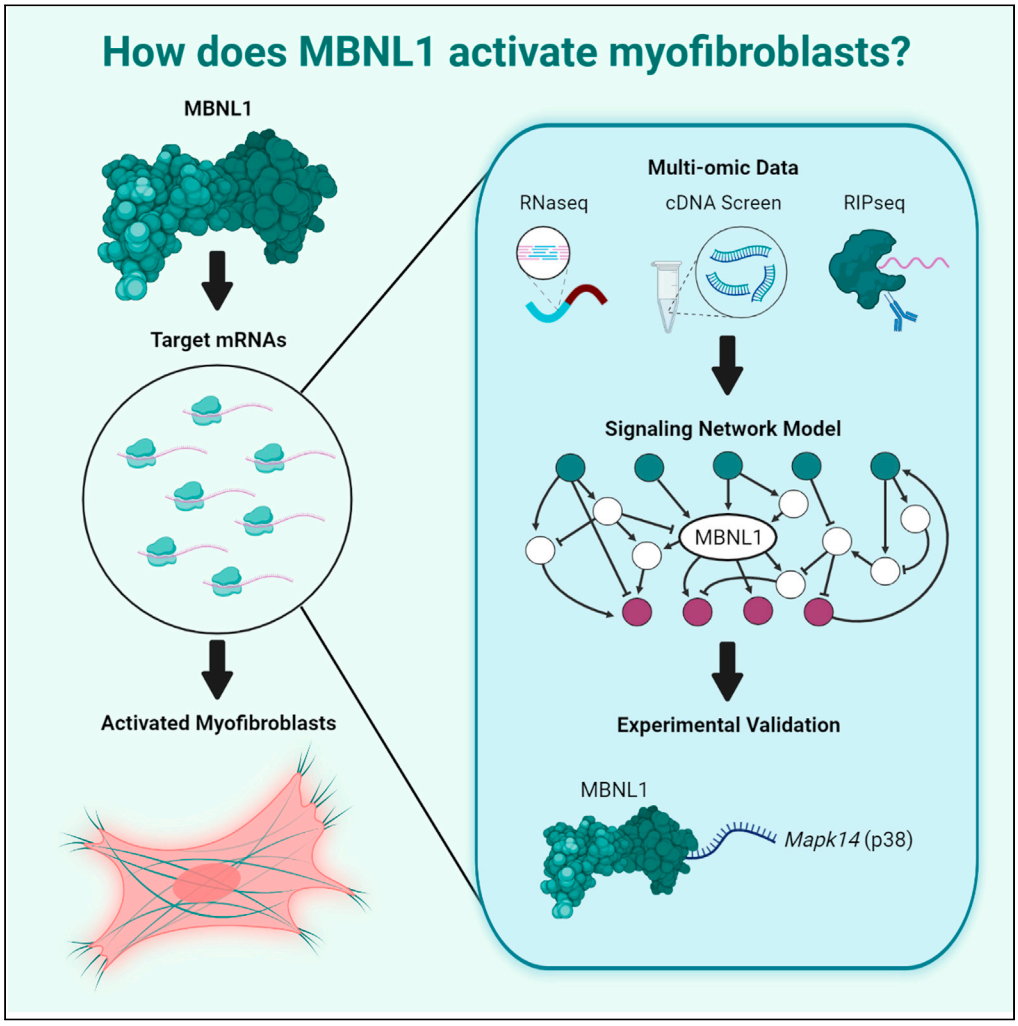

Anders R. Nelson, Darrian Bugg, Jennifer Davis, Jeffrey J. Saucerman

jsaucerman@virginia.edu

Highlights

Integrated model predicts MBNL1 signaling targets affecting myofibroblast activation

Predicted that MBNL1 targets drive myofibroblast activation via redundant signaling

Predicted MBNL1 regulatory mechanisms for Hippo, Runx, Sox9, and p38 pathways

MBNL1 knockdown reduces p38 protein expression in mouse cardiac fibroblasts

Nelson et al., iScience 26, 106502
April 21, 2023 © 2023
https://doi.org/10.1016/j.isci.2023.106502

iScience

CellPress
OPEN ACCESS

Article

Network model integrated with multi-omic data predicts MBNL1 signals that drive myofibroblast activation

Anders R. Nelson,[1] Darrian Bugg,[2] Jennifer Davis,[2,3,4] and Jeffrey J. Saucerman[5,6,*]

SUMMARY

RNA-binding protein muscleblind-like1 (MBNL1) was recently identified as a central regulator of cardiac wound healing and myofibroblast activation. To identify putative MBNL1 targets, we integrated multiple genome-wide screens with a fibroblast network model. We expanded the model to include putative MBNL1-target interactions and recapitulated published experimental results to validate new signaling modules. We prioritized 14 MBNL1 targets and developed novel fibroblast signaling modules for p38 MAPK, Hippo, Runx1, and Sox9 pathways. We experimentally validated MBNL1 regulation of p38 expression in mouse cardiac fibroblasts. Using the expanded fibroblast model, we predicted a hierarchy of MBNL1 regulated pathways with strong influence on αSMA expression. This study lays a foundation to explore the network mechanisms of MBNL1 signaling central to fibrosis.

INTRODUCTION

Heart failure complications following many forms of cardiac injury, including myocardial infarction (MI), are closely linked to a fibrotic wound healing response.[2] This process is primarily mediated by activated myofibroblasts. These cells exhibit contractile behavior and robust deposition of extracellular matrix (ECM) proteins in response to profibrotic cytokines including TGF-β.[3] Myofibroblast activation is canonically regulated by the TGF-β/Smad2-3 axis, as well as renin-angiotensin-aldosterone signaling and non-canonical TGF-β signaling via p38 MAP kinase, TRPC6, and PI3K/Akt, and mechanical stress signaling via Rho kinases and MRTF and serum response factor (SRF).[4–9] Although these pathways lay a framework for fibroblast regulation of ECM, greater knowledge of fibroblast signaling is necessary to develop effective therapeutic strategies for fibrosis.[3,10]

Recently, we identified RNA-binding protein muscleblind-like1 (MBNL1) as a central regulator of post-MI cardiac wound healing and myofibroblast activation in mice, as well as of renal and pulmonary fibrosis.[1] We showed that MBNL1 regulates myofibroblast activation by modulating SRF and calcineurin Aβ (CnAβ) mRNA stability and splicing respectively. Although these findings indicate an important role for fibroblast MBNL1 signaling during wound healing, MBNL1 omics data including RNA-seq and RIPseq (RNA immunoprecipitation followed by RNA-seq) suggest that MBNL1 signals via multiple other pathways including non-canonical TGF-β, p38 MAPK, and growth factor pathways.[1] Mapping MBNL1 signaling in fibroblasts will aid in identifying novel fibrotic regulators and predicting signaling mechanisms. A major challenge in omics analysis is prioritizing influential regulators from lists of candidates. Further, although general best practices are established for individual data analyses, there is not a standard practice for integrating multi-omics datasets to identify disease targets.[11–13]

Integrated network analysis approaches have become an increasingly powerful choice for prioritizing candidate regulators in genome-wide studies.[14,15] Our group has previously used large-scale computational models to identify regulatory linchpins for cardiac signaling, including fibroblast activation and fibrosis.[16–18] Here, we combined omics data mining and network modeling to map MBNL1 signaling in fibroblasts and predict regulators of cardiac wound healing. Using the expanded fibroblast network model, we screened for putative MBNL1 targets that drive αSMA expression and predicted signaling mechanisms for these regulators. We predicted and experimentally validated MBNL1's role in p38 MAPK expression in cardiac fibroblasts.

[1]Department of Pharmacology, University of Virginia, 1340 Jefferson Park Avenue, Pinn Hall, 5th Floor, PO Box 800735, Charlottesville, VA 22908-0735, USA

[2]Department of Lab Medicine & Pathology, University of Washington, 1959 NE Pacific Street Box 357470, Seattle, WA 98195, USA

[3]Department of Bioengineering, University of Washington, PO Box 355061, Seattle, WA 98195-5061, USA

[4]Institute for Stem Cell & Regenerative Medicine, University of Washington, 850 Republican Street, PO Box 358056, Seattle, WA 98109, USA

[5]Department of Biomedical Engineering, University of Virginia, PO Box 800759, Charlottesville, VA 22903 , USA

[6]Lead contact

*Correspondence: jsaucerman@virginia.edu

https://doi.org/10.1016/j.isci.2023.106502

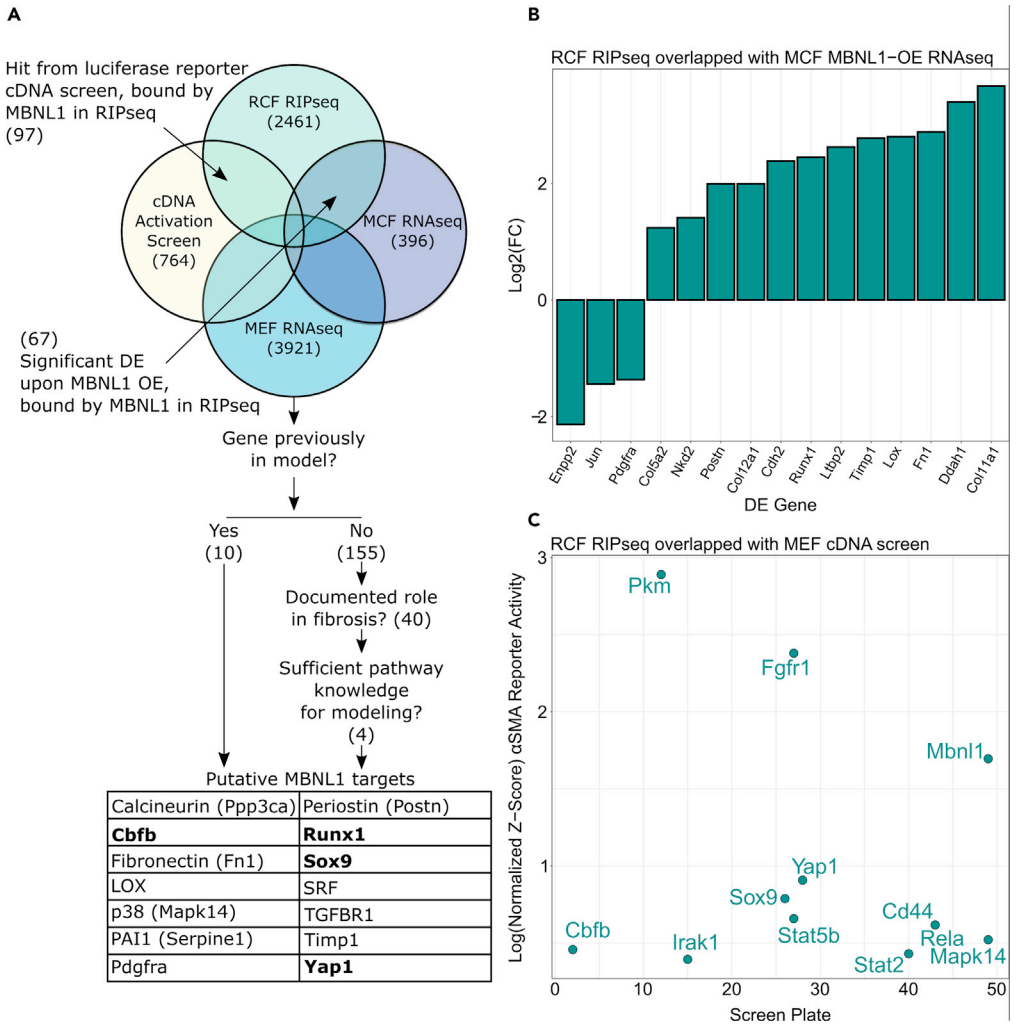

Figure 1. Candidate MBNL1 regulatory targets identified through multi-omic integration

(A) Omics data overlap approach to identify putative MBNL1 target mRNAs. Priority overlaps are labeled with arrows in the Venn diagram. Genes added to the network model are bolded.

(B) Select genes with high relevance to fibrosis from rat cardiac fibroblast (RCF) RIPseq overlapped with MCF RNA-seq. These genes are bound by MBNL1 and exhibit expression driven by MBNL1 in mouse cardiac fibroblasts.

(C) Select genes with high relevance to fibrosis from RCF RIPseq overlapped with MEF cDNA *Acta2* promoter-reporter screen. These genes are bound directly by MBNL1 and can drive αSMA expression when overexpressed. Also see Figures S1.

RESULTS

A genome-wide screen identifies drivers of αSMA promoter activity

To identify drivers of myofibroblast activation, we developed a computational pipeline to reanalyze a genome-wide screen for cDNAs that increase αSMA promoter activity in mouse embryonic fibroblasts (MEFs).[1] Previously, this cDNA screen was used to identify MBNL1 as a putative fibrotic regulator.[1] Here, our normalization approach allowed screen hits to be compared across plates to determine genome-wide screen hits. Gene set enrichment of hits showed significant membership for adherens junction formation, calcium signaling, multiple RNA regulation terms, Hippo pathway signaling, and many terms related to increased metabolism[19] (Figure S3). Although some of these gene sets are expected to induce an activated myofibroblast state, Hippo signaling genes, including *Yap1*, were of particular interest given the recent identification of *Yap1* as a wound healing regulator[20,21] (Figure 1A). Furthermore, the enrichment of transcript misregulation genes in our hit list supports the role of RNA modifying proteins like MBNL1 as major players in myofibroblast activation[22] (Figure S3).

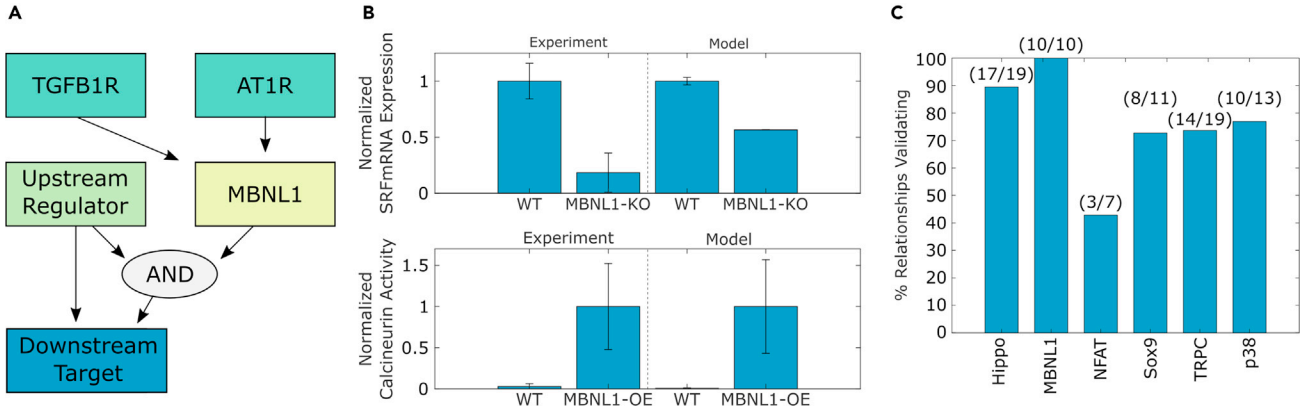

Figure 2. Network model maps MBNL1 regulations of target mRNAs

(A) Model implementation for MBNL1 signaling to downstream targets. Upstream regulators can partially activate downstream MBNL1 targets, but require the presence of MBNL1 for complete target activation.

(B) Model validation against two experimental results from our previous study.[1] (Top) SRFmRNA is partially diminished on MBNL1 knockout following MI, represented by high TGFβ and AngII in the model.[18] (Bottom) MBNL1 overexpression drives Calcineurin activity.

(C) Experimental validation of 79 intermediate-output relationships from the literature, grouped by signaling module. Data is represented as mean ± S.E.M. Also see Figure S2.

A computational model of MBNL1 signaling to fibrotic regulatory targets

MBNL1 was previously shown to modulate mRNAs for calcineurin A β, SRF, and TGFβR2.[1] The *in vitro* mouse embryonic fibroblast (MEF) RNA-seq and rat cardiac fibroblast (RCF) RIPseq datasets by Davis et al. suggest many additional candidate targets for MBNL1 regulation in fibroblasts.[1] RNA-seq studies following MBNL1 knockdown demonstrate that MBNL1 promotes differentiated cell states through regulation of many target RNAs, and that MBNL1 is necessary for differentiation.[23,24] These data together support a broad and central signaling role for MBNL1 in myofibroblast activation. To determine if MBNL1 binds known regulators for fibrosis, we compared genes from the published MBNL1-OE RNA Immunoprecipitation sequencing (RIPseq) with genes from the most recent version of our fibroblast network model.[1,18] MBNL1 bound 42 mRNAs and modulated 3 mRNAs corresponding to 45 nodes (~40%) in the fibroblast model (Table S1), indicating that this network model would be a useful tool to map MBNL1 signaling.

Candidate MBNL1 regulatory targets that were not members of the fibroblast network model were manually curated by literature review to determine if the target could fit in a putative signaling pathway related to fibrosis or differentiation. As the genome-wide cDNA screen only identifies positive, but not negative, regulators of αSMA, we focused on identifying profibrotic regulators downstream of MBNL1. We prioritized genes from two data overlap categories: Genes bound by MBNL1 in RIPseq that showed increased differential expression in mouse cardiac fibroblast (MCF) RNA-seq on *in vivo* MBNL1 overexpression (67 genes) (Figures 1B and S1A); and genes bound by MBNL1 in RIPseq that were hits in the cDNA screen (97 genes) (Figures 1C and S1B) (DataS1). All modeled MBNL1 targets except for PAI1 (*Serpine1*) were in these first-priority overlaps. We filtered the candidate list to 60 genes that were not members of the model and determined that 4 of these genes (*Sox9*, *Runx1*, *Yap1*, and *Cbfb*) had sufficient pathway knowledge to incorporate in the cardiac fibroblast network model. From our list of candidates, we identified 10 MBNL1 targets already in the network model. Including SRF, CnA, and TGFβR1, there are 14 MBNL1 targets in the network model (Figure 1A). The complete integrated network model schematic is shown in Figure S5.

Validation of predictive model accuracy

To map MBNL1 signaling in fibroblasts, we expanded the cardiac fibroblast network with MBNL1 signaling reactions to these 14 targets and added new pathways for 7 of these targets (Figure 2A). As a test of the predictive capacity of the model for MBNL1 signaling, we simulated two experiments from our previous study,[1] showing the model predicted similar changes in SRF and calcineurin mRNA as those observed in our fibroblast experiments on MBNL1 perturbation (Figure 2B).

We next expanded our model validation tests to more systematically determine the accuracy of the MBNL1 fibroblast network model, using experimental data from recent fibrosis studies *in silico*. Input-Output

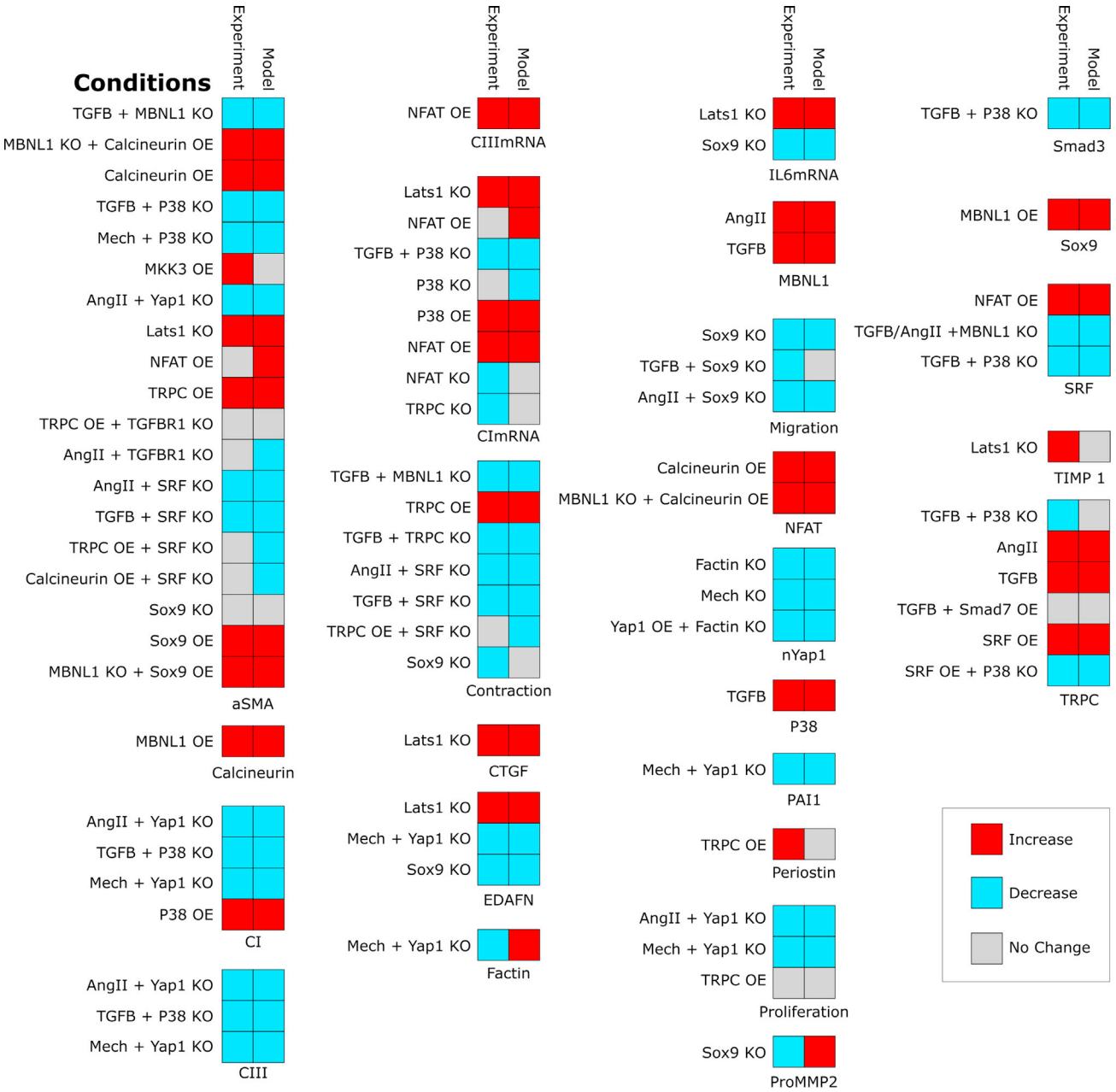

Figure 3. Validation relationships of the MBNL1 fibroblast network model for Input-Output validations curated from the literature

Colored boxes represent cases of 'Increase', 'Decrease' or 'No Change' on a given perturbation. Validation relationships are categorized by the measured output. OE and KO stand for overexpression and knockout respectively. Also see Figure S4.

validations were performed as described previously.[17] Here, previously published experiments were simulated and predicted results were compared to those of *in vitro* experiments. Model-predicted phenotypic outputs such as 'Proliferation' are determined by measuring activity of the respective network node (Figure S5). Model and experimental results were compared qualitatively, observing if the output of interest increased, decreased, or showed no significant change on perturbation. These validations contain experiments where an input is elevated and an output is measured (i.e. elevated TGFβ increases Col1). The model validated against 80% (66/83) of Input-Output relationships (Figure S4).

To recapitulate perturbation experiments relevant to the new MBNL1-target interactions in the model, we created a table of 79 Intermediate-Output validations (Figure 3). Intermediate-Output validations include

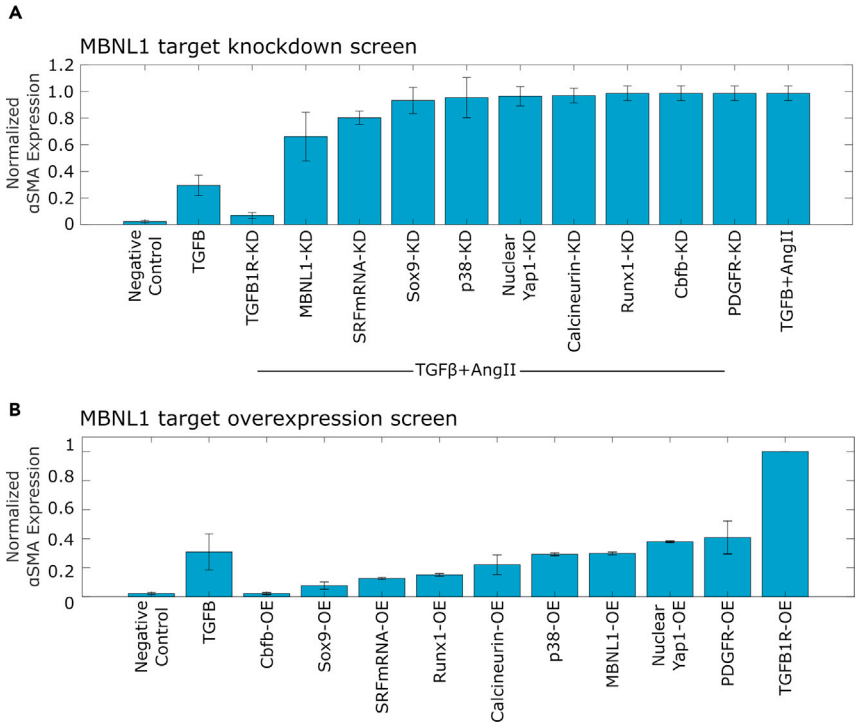

Figure 4. Expanded model predicts effects of MBNL1 target signaling perturbations on αSMA

(A) αSMA expression on simulated knockdown of MBNL1 targets in the context of high TGFβ+AngII.

(B) αSMA expression in response to simulated overexpression of MBNL1 and its targets. Values in panels A and B are model predictions normalized to the same scale, where 1 is maximal possible αSMA. Data is represented as mean ± S.E.M.

experiments with intracellular perturbation (i.e. p38 OE increases α-SMA) whereas Input-Output validations include extracellular signaling outcomes (i.e. TGFβ treatment increases Col1 mRNA). Intermediate-Output model predictions validated against 78% (62/79) of Intermediate-Output validations (Figures 2C and 3). Validation percentages were highest for experiments perturbing MBNL1, Hippo, and p38 MAPK signaling.

Virtual perturbation screens for MBNL1 target influence on αSMA expression

To determine which modeled MBNL1 targets are most influential in activating αSMA expression, we simulated systematic knockdown of MBNL1 targets (Figure 4A). We expect αSMA activity to be low in quiescent cells, and high during cardiac injury. Therefore, we screened for αSMA expression-driving MBNL1 targets in a simulated AngII+TGFβ signaling context, as AngII and TGFβ increase MBNL1 expression.[1] SRF showed the most influence on knockdown, whereas Sox9 and calcineurin, two validated MBNL1 targets, were not as influential as regulators of αSMA.[1,25] Of interest, Runx1 and Cbfb had negligible effects on αSMA expression on simulated knockdown. To complement knockdown simulations, we further tested the role of MBNL1 target overexpression on αSMA promoter activity (Figure 4B). Here, as in the cDNA screen, simulated overexpression of most MBNL1 targets showed robust increases in αSMA similar to that of MBNL1-OE. TGFβ1R-OE had a greater effect, consistent with it being a highly recognized activator of fibrotic signaling.[26] These predictions are congruent with experimental studies showing that Sox9, Yap1, and p38 regulate post-MI wound healing and αSMA expression.[25,27–29] The combined results from these screens suggest that loss-of-function in MBNL1 targets can be partially compensated for by other targets to conduct profibrotic MBNL1 signaling, but MBNL1 targets individually can be sufficient to drive αSMA expression when their activity is elevated. It is also possible that profibrotic signaling for some of these targets is not fully captured by the model. For example, it is likely that Sox9 directly regulates the promoter of a *Col1* gene, as it shows a similar function on the *Col2a1* promoter in chondrocytes and colocalizes with Col1 protein *in vivo*, but insufficient information is available currently to include this mechanism in our model.[29–31]

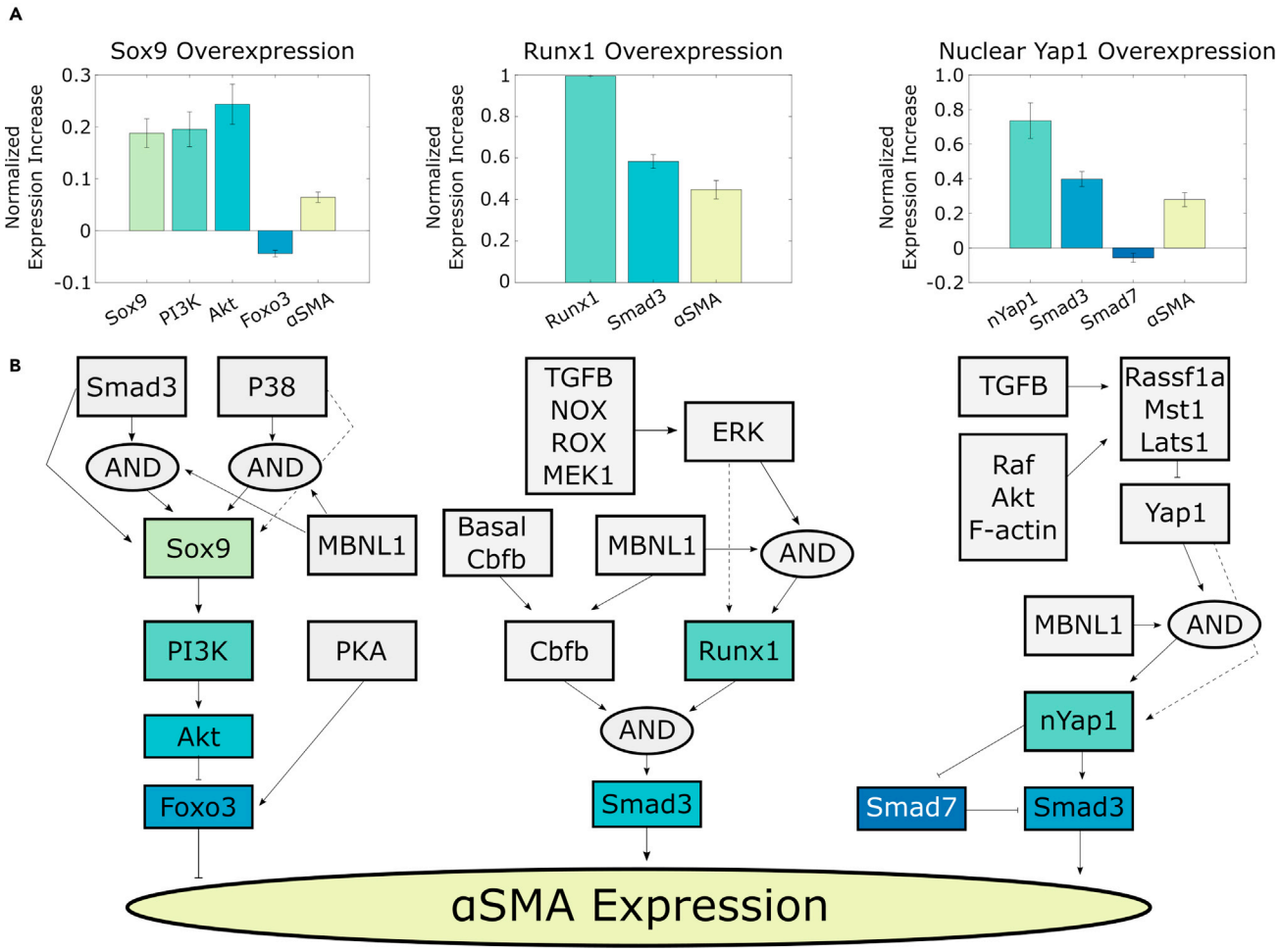

Figure 5. Simulated overexpressions predict signaling mechanisms of MBNL1 targets

(A) Normalized expression changes predicted by the model for select nodes downstream of Sox9, Runx1, and Nuclear Yap1.

(B) Schematics representing signal transduction from MBNL1 targets to αSMA expression. Colored nodes correspond to measured nodes in panel A. Data is represented as mean ± S.E.M.

Recently, we determined that p38 regulates Yap signaling in fibroblasts.[32] This finding is further supported by these computational screens where p38 and Yap1 are both predicted to conduct profibrotic MBNL1 signaling (Figure 4B). The PI3K/Akt axis was recently shown to have a regulatory role in fibrosis.[33] Notably, Sox9 and p38 are modeled to signal via this pathway and also increase Hippo signaling through the inhibition of Mst1 via Akt. Runx1/Cbfb and Yap1 also signal via the canonical Smad3 axis. This network model supports a framework where influential fibrosis regulators converge on shared pathways while maintaining some independent influence on downstream αSMA expression. Our simulation results imply that cardiac fibrosis is dependent on a network of interconnected regulators instead of isolated independent pathways and that these regulators are transcriptionally controlled by MBNL1.

Putative signaling pathways for novel regulators of fibrosis

Next, we applied the MBNL1-incorporated fibroblast signaling network model to determine predicted signaling pathways for putative MBNL1 targets nuclear Yap1, Sox9, Runx1, and p38. To investigate how targets signal to αSMA downstream of MBNL1, we simulated overexpression of MBNL1 targets in a high MBNL1 context and tracked activation of nodes between the overexpressed target and αSMA.

Simulated Sox9 overexpression was predicted to increase the activity of PI3K and Akt, and to decrease activity for Foxo3 (Figure 5A). As Foxo3 suppresses αSMA and Collagen expression, these simulation

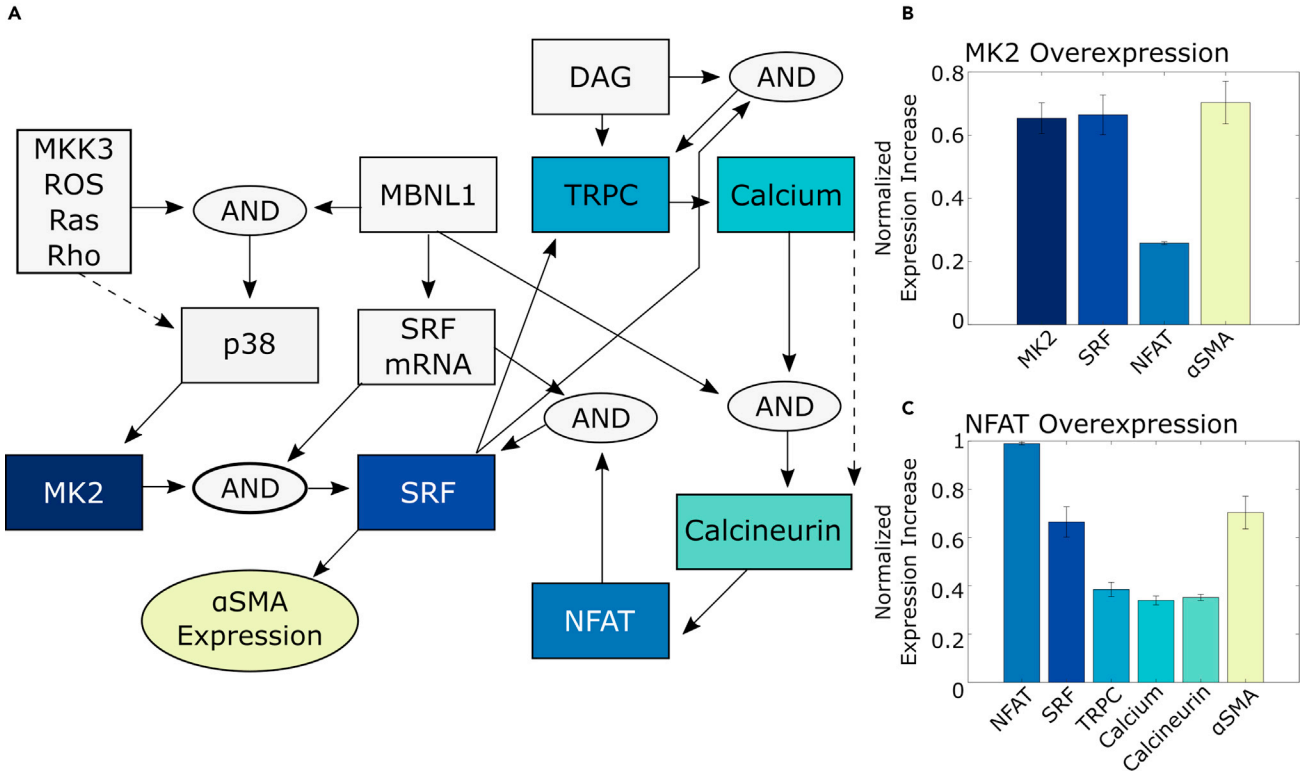

Figure 6. Simulated overexpressions predict p38 signaling via MK2 and an NFAT-SRF feedback loop

(A) Schematic representing p38 signaling to αSMA through MK2 directly via SRF, and indirectly via NFAT feedback to SRF. Nodes are colored for identification to match panels B and C.

(B) Model-predicted normalized expression changes for select nodes downstream of MK2. MK2 overexpression was simulated to track signaling propagation of downstream p38 signaling.

(C) Normalized expression changes for select nodes downstream of NFAT. NFAT expression was predicted to increase under MK2 overexpression. NFAT overexpression was simulated to determine if MK2 can activate αSMA via NFAT. Data is represented as mean ± S.E.M.

results support a predicted signaling pathway where Sox9 drives expression of PI3K and Akt resulting in suppression of antifibrotic Foxo3.

As Cbfb has been shown to bind and stabilize Runx proteins, it is often necessary for full Runx family protein expression and function. Therefore, we simulated Runx1 overexpression with a basal input of Cbfb to map Runx1 signaling without being limited by Cbfb availability.[34–36] The simulated overexpression resulted in increased Smad3 activity (Figure 5A). Here, we predict that Runx1 and Cbfb activate Smad3 directly, leading to increased αSMA expression. This pathway also forms a direct connection between MBNL1 and canonical fibrotic regulator Smad3.

Next, we simulated overexpressed nuclear Yap1, a central transcription factor to the Hippo pathway and a putative MBNL1 target. Nuclear Yap1 OE was predicted to simultaneously increase Smad3 activity and decrease Smad7 activity (Figure 5A). As Smad7 inhibits Smad3 activity, nuclear Yap1 is predicted to increase αSMA expression by activating Smad3 directly, and by blocking the activity of Smad7, further increase Smad3 activity.

P38 signals through multiple pro- and antifibrotic pathways in our model. MK2 inhibition, downstream of p38, has been shown to mitigate post-MI fibrosis in mice.[37] We simulated overexpression of MK2 to map an isolated profibrotic branch of p38 signaling. Simulated MK2 overexpression was predicted to increase the expression of αSMA, as well as for activity of SRF and NFAT (Figure 6B). We next wanted to determine if profibrotic p38 signaling was occurring solely through SRF, or if NFAT signaling was also predicted to play a role in αSMA expression. We simulated NFAT overexpression and predicted increased activity for SRF, TRPC, calcium, and calcineurin (Figure 6C). From these results, we predict that p38, via

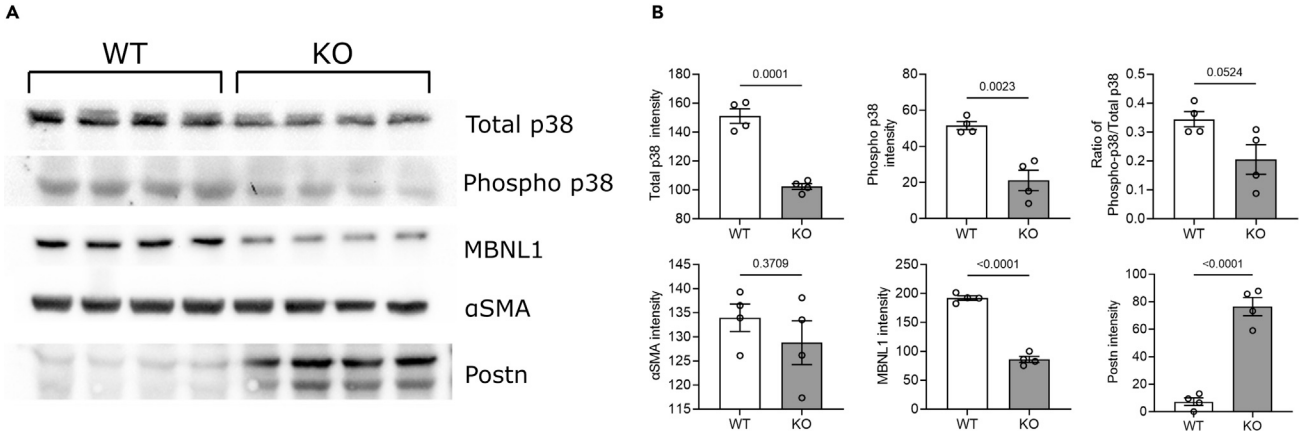

Figure 7. As predicted by the model, MBNL1 knockout in adult mouse cardiac fibroblasts reduces expression of p38

(A) Western blot of mouse cardiac fibroblasts from adenoviral Cre-treated mice (KO) and those with normal MBNL1 expression (WT). Proteins run on individual gels.

(B) Quantification of western blot data, pvalues from Student's t-test listed above bars. Data is represented as mean ± S.E.M. Also see Figures S6 and S7.

MK2, increases expression of αSMA directly via SRF, and p38 also activates the TRPC/calcineurin/NFAT pathway that further increases αSMA expression via positive feedback activation of SRF. Although MBNL1 regulation of SRF mRNA was previously shown, MBNL1's predicted regulation of p38 expression is a novel role for MBNL1. We next aimed to validate the MBNL1-p38 signaling relationship with experiments in mouse cardiac fibroblasts.

Experimental validation of predicted MBNL1-p38 MAPK interaction

To determine if MBNL1 regulates p38 expression as predicted by the model, we treated adult cardiac fibroblasts from MBNL1-floxed mice with Cre to induce MBNL1 knockout. Western blot results show a reduction in p38 and phospho-p38 in Cre-treated fibroblasts compared to the wild-type fibroblasts (Figure 7), validating the model prediction. Expression of fibrotic marker proteins αSMA and periostin did not significantly decrease on MBNL1 KO, and periostin expression increased. Reduction in both p38 and phospho-p38 forms on MBNL1 knockout indicates that MBNL1 is necessary for the full expression and activity of p38 (Figure 7). Complete western blot gels are shown in Figure S7.

DISCUSSION

Omics-integrated model for MBNL1 fibroblast signaling

MBNL1 is increasingly recognized as a central regulator of fibrosis, but its downstream regulatory mechanisms are not well characterized. The fibroblast network model was previously used to predict signaling interactions across a broad range of fibrosis regulatory pathways. Here, we aimed to expand and repurpose this model to predict MBNL1 target interactions leading to fibroblast activation.[18] We used multi-omic data to expand a fibroblast network model including MBNL1 and its putative targets. The expanded model was validated at a rate of 78% (62/79) against independently published perturbation experiments. The model predicted the relative influence of MBNL1 targets on αSMA expression during overexpression and knockdown and predicted signaling mechanisms for Hippo, Runx, Sox9, and p38 pathways conducting MBNL1 signaling to αSMA. Model-predicted MBNL1 regulation of its target p38 MAPK was experimentally validated in mouse cardiac fibroblasts.

Convergence and redundancy of MBNL1 target signaling

Fibrotic signal transduction involves many input pathways that often converge on key hubs.[3] In overexpression simulations for putative MBNL1 targets, we showed that both Runx1 and Yap1 converged on Smad3 to modulate αSMA (Figure 5). P38, another MBNL1 target confirmed experimentally, converged on SRF to modulate αSMA (Figure 6). The convergence of fibrotic regulators on signaling hubs creates signaling redundancy that makes it challenging to distinguish the most influential regulators of fibrosis. In our knockdown and overexpression simulations (Figure 4), we showed that knockdown of most MBNL1 targets caused only small decreases in αSMA expression in a high AngII+TGFβ context. However, the

overexpression simulations predicted much greater absolute changes in αSMA expression than in the knockdown. From these results, we predict MBNL1 targets have a high impact on fibrosis when activated individually, but partially compensate for one another when knocked out. Consistent with these predictions, we have previously shown that overexpression of MKK6 upstream of p38 can directly drive myofibroblast activation and cardiac fibrosis in mice.[28] Yap1, another putative MBNL1 target, was recently shown to drive post-MI fibrosis when overexpressed.[38] Future studies on MBNL1 signaling could examine the effects of crosstalk and signaling redundancy between MBNL1 targets during wound healing.

The broad scope of MBNL1 regulation across fibroblast pathways

We used an overlap strategy to filter hits from omics studies down to 256 candidate regulators. We found that 60 of these genes had a documented role in cardiac fibrosis, and it is likely that some of these candidate genes play a significant role in fibrosis downstream of MBNL1. Candidates were only incorporated in the model if their fibroblast signaling pathways were well characterized and could be connected to downstream αSMA expression. Although only 14 targets were included in the signaling network model, the other candidates should be considered in future work on cardiac wound healing.

Of the unincorporated candidates, there are four that stand out with particular clinical relevance for cardiac fibrosis. Irak1, part of the TLR/IL-1 signaling cascade, has been implicated in multiple fibrotic diseases.[39] The IL-1 receptor is also a therapeutic target for anakinra (Kineret), a recent candidate therapy for MI patients currently in phase 2 clinical trials (NCT01175018).[40,41] Nkd2 is a documented antagonist of Wnt signaling in cancer.[42] Canonical Wnt signaling plays a role in cardiac fibrosis through multiple pathways including calcium signaling to promote cellular activation and proliferation.[43] Cd44 was recently shown to be a critical regulator of cardiac wound healing in mice.[44] Cd44 deficiency was further shown to mimic AT1R inhibition during AngII-induced cardiac fibrosis, reducing macrophage migration, myofibroblast proliferation, and interstitial fibrosis.[45] Latent transforming growth factor binding protein 2 (Ltbp2) is responsible for binding secreted TGFβ to the extracellular matrix. Ltbp2 is upregulated in fibroblasts during dilated cardiomyopathy, and Ltbp2 siRNA reduced pathological remodeling.[46] Indeed, regulation of fibroblast latent TGFβ signaling is a priority target for the development of antifibrotic therapeutics.[47] Future studies could investigate a role for MBNL1 in regulating mRNAs of these candidate genes.

Model validation

We curated a new set of published validation experiments to test the predictive accuracy of the expanded network model. This new validation set comprises Intermediate-Output experiments where MBNL1 and its putative targets are perturbed and cellular outputs are measured. The model validated against 78% (62/79) of relationships. The validation subsets that have the highest percentage of failures are NFAT (4), TRPC (8), and p38 (4). Half of these relationships are instances where no significant change was shown in an experiment, but a significant change in node activity was seen in the model prediction. One explanation for this is that our number of ensemble simulations is higher than the typical number of biological replicates in *in vitro* studies. Lower replicate number in *in vitro* studies may lack sufficient statistical power to detect small changes.

Other failed validations can guide future model revisions and experiments. For example, although it has been shown that increased TRPC increases expression of periostin, our model does not connect TRPC6 to periostin.[5] In this model, most of TRPC's profibrotic signaling is conducted through NFAT and SRF. To our knowledge, no study has shown that SRF regulates periostin in cardiac fibroblasts. Although previous studies have shown that perturbations to SRF and MRTF signaling in myocytes affect periostin expression, the fibroblast-specific mechanisms of TRPC signaling in periostin regulation should be further explored.[48,49]

In our *in vitro* validation experiment with adult mouse primary cardiac fibroblasts, expression of the activation marker αSMA did not significantly decrease on MBNL1 KO. This result is different than our previous study in TGFβ-treated mouse embryonic fibroblasts, where MBNL1 KO reduced αSMA expression.[1] Activation of adult mouse primary cardiac fibroblasts is highly sensitive to mechanical tension.[50–52] It is likely that these cardiac fibroblasts cultured on a rigid substrate were activated via mechanical stress signaling pathways independent of MBNL1, causing αSMA expression in the MBNL1 KO condition. Although we expected periostin expression to decrease on MBNL1 KO, its expression increased. Given that MBNL1 binds and directly regulates many mRNAs, it is possible that MBNL1 positively regulates mRNAs for genes that

negatively regulate periostin expression, and that MBNL1 knockout reduced the expression of these negative regulators.

Limitations of the study

Our network model's primary limitations are the use of default parameters and that it is currently best suited for *in vitro* environments where the inputs are well defined. As seen in previous studies, our network models, including a previous version of this fibroblast network model, are robust to parameter variation.[17,53] Here, we also improved the simulation robustness using an ensemble approach described above. With this approach, we randomly sampled model parameters within a normal distribution over many simulations to make consensus model predictions. The original fibroblast network model was built on a body of literature on well-studied and canonical fibroblast pathways.[17] Literature for this expanded model was more limited, as it pertains to novel non-canonical fibrotic regulators. We have identified a set of many putative regulators that can be adapted to improve this model as more published data becomes available.

Limitations of the experimental system may also contribute to interpretation of model validation. In our validation experiment in cardiac fibroblasts, we observed incomplete knockout of MBNL1 because of limitations of adenoviral transfection efficiency at 500 MOI, which is optimized for cell health. The decrease in p38 expression is consistent with the degree of decreased MBNL1 expression in the adeno-Cre treated cells. This indicates that the observed expressions of alpha-SMA and periostin are more likely because of mechanical activation than because of non-transduced cells.

We developed an expanded fibroblast network model integrated with genome-wide data to map MBNL1 signaling across 14 targets in cardiac fibroblasts. Simulated knockdown and overexpression screens predicted MBNL1 targets exhibit partially redundant signaling when knocked out but are sufficient to drive αSMA expression when overexpressed. By simulating overexpression of individual MBNL1 targets and tracing node expression, we predicted signaling mechanisms for MBNL1 targets Yap1, Runx1, Sox9, and p38. We predicted that MBNL1 regulates p38 MAPK, and validated this relationship with experiments in cardiac fibroblasts. The data overlap and network modeling approaches used here enabled identification and mechanistic predictions for targets of MBNL1 during cardiac fibrosis.

STAR★METHODS

Detailed methods are provided in the online version of this paper and include the following:

- KEY RESOURCES TABLE
- RESOURCE AVAILABILITY
  - Lead contact
  - Materials availability
  - Data and code availability
- EXPERIMENTAL MODEL AND SUBJECT DETAILS
- METHOD DETAILS
  - Analysis of a genome-wide cDNA αSMA reporter luciferase screens
  - Data overlap and putative MBNL1 target prioritization
  - First priority overlaps
  - Second priority overlaps
  - Fibroblast network model expansion with MBNL1
  - Model simulations
  - Model validation
  - Perturbation screens for MBNL1 target influence on αSMA expression
  - Overexpression simulations to investigate MBNL1 target signaling mechanisms
  - *In vitro* experiments
  - Western blot
- QUANTIFICATION AND STATISTICAL ANALYSIS

SUPPLEMENTAL INFORMATION

Supplemental information can be found online at https://doi.org/10.1016/j.isci.2023.106502.

ACKNOWLEDGMENTS

This work was supported by grants from the National Institutes of Health for JD [grants numbers HL141187 & HL142624] and JS [grant numbers HL137755 & HL160665], the NIH Biological Mechanisms of Healthy Aging Training Program [grant number T32AG066574] and Cardiovascular Research Training Program (NIH T32 HL007828) for DB, and the NIH Basic Cardiovascular Research Training Program for AN [grant number T32HL007284].

AUTHOR CONTRIBUTIONS

Conceptualization, A.N., J.S., and J.D.; Methodology, A.N. and D.B.; Software, A.N.; Investigation, A.N. and D.B.; Formal Analysis, A.N. and D.B; Writing – Original Draft, A.N. and J.S.; Writing – Review & Editing, A.N., J.S., D.B., and J.D.; Funding Acquisition, J.S., J.D., A.N., and D.B.; Resources, J.S. and J.D.; Data Curation, A.N., J.S., and J.D.; Supervision, J.S. and J.D.; Visualization, A.N. and D.B.

DECLARATION OF INTERESTS

The authors declare no competing interests.

Received: May 19, 2022
Revised: January 9, 2023
Accepted: March 23, 2023
Published: March 27, 2023

REFERENCES

1. Davis, J., Salomonis, N., Ghearing, N., Lin, S.-C.J., Kwong, J.Q., Mohan, A., Swanson, M.S., and Molkentin, J.D. (2015). MBNL1-mediated regulation of differentiation RNAs promotes myofibroblast transformation and the fibrotic response. Nat. Commun. *6*, 10084. https://doi.org/10.1038/ncomms10084.

2. Francis Stuart, S.D., De Jesus, N.M., Lindsey, M.L., and Ripplinger, C.M. (2016). The crossroads of inflammation, fibrosis, and arrhythmia following myocardial infarction. J. Mol. Cell. Cardiol. *91*, 114–122. https://doi.org/10.1016/j.yjmcc.2015.12.024.

3. Ma, Z.-G., Yuan, Y.-P., Wu, H.-M., Zhang, X., and Tang, Q.-Z. (2018). Cardiac fibrosis: new insights into the pathogenesis. Int. J. Biol. Sci. *14*, 1645–1657. https://doi.org/10.7150/IJBS.28103.

4. Turner, N.A., Das, A., Warburton, P., O'Regan, D.J., Ball, S.G., and Porter, K.E. (2009). Interleukin-1α stimulates proinflammatory cytokine expression in human cardiac myofibroblasts. Am. J. Physiol. Heart Circ. Physiol. *297*, H1117–H1127. https://doi.org/10.1152/ajpheart.00372.2009.

5. Davis, J., Burr, A.R., Davis, G.F., Birnbaumer, L., and Molkentin, J.D. (2012). A TRPC6-dependent pathway for myofibroblast transdifferentiation and wound healing in vivo. Dev. Cell *23*, 705–715. https://doi.org/10.1016/j.devcel.2012.08.017.

6. Bujak, M., and Frangogiannis, N.G. (2007). The role of TGF-β signaling in myocardial infarction and cardiac remodeling. Cardiovasc. Res. *74*, 184–195. https://doi.org/10.1016/j.cardiores.2006.10.002.

7. Parmacek, M.S. (2010). Myocardin-related transcription factor-a: mending a broken heart. Circ. Res. *107*, 168–170. https://doi.org/10.1161/CIRCRESAHA.110.224881.

8. AlQudah, M., Hale, T.M., and Czubryt, M.P. (2020). Targeting the renin-angiotensin-aldosterone system in fibrosis. Matrix Biol. *91–92*, 92–108. https://doi.org/10.1016/J.MATBIO.2020.04.005.

9. Velasquez, L.S., Sutherland, L.B., Liu, Z., Grinnell, F., Kamm, K.E., Schneider, J.W., Olson, E.N., and Small, E.M. (2013). Activation of MRTF-A-dependent gene expression with a small molecule promotes myofibroblast differentiation and wound healing. Proc. Natl. Acad. Sci. USA *110*, 16850–16855. https://doi.org/10.1073/PNAS.1316764110/-/DCSUPPLEMENTAL.

10. Travers, J.G., Tharp, C.A., Rubino, M., and McKinsey, T.A. (2022). Therapeutic targets for cardiac fibrosis: from old school to next-gen. J. Clin. Invest. *132*, e148554. https://doi.org/10.1172/JCI148554.

11. Subramanian, I., Verma, S., Kumar, S., Jere, A., and Anamika, K. (2020). Multi-omics data integration, interpretation, and its application. Bioinf. Biol. Insights *14*, 1177932219899051. https://doi.org/10.1177/1177932219899051.

12. Canzler, S., Schor, J., Busch, W., Schubert, K., Rolle-Kampczyk, U.E., Seitz, H., Kamp, H., von Bergen, M., Buesen, R., and Hackermüller, J. (2020). Prospects and challenges of multi-omics data integration in toxicology. Arch. Toxicol. *94*, 371–388. https://doi.org/10.1007/s00204-020-02656-y.

13. Conesa, A., Madrigal, P., Tarazona, S., Gomez-Cabrero, D., Cervera, A., McPherson, A., Szcześniak, M.W., Gaffney, D.J., Elo, L.L., Zhang, X., and Mortazavi, A. (2016). A survey of best practices for RNA-seq data analysis. Genome Biol. *17*, 13–19. https://doi.org/10.1186/s13059-016-0881-8.

14. Altaf-Ul-Amin, M., Afendi, F.M., Kiboi, S.K., and Kanaya, S. (2014). Systems biology in the context of big data and networks. BioMed Res. Int. *2014*, 428570. https://doi.org/10.1155/2014/428570.

15. Oulas, A., Minadakis, G., Zachariou, M., Sokratous, K., Bourdakou, M.M., and Spyrou, G.M. (2019). Systems Bioinformatics: increasing precision of computational diagnostics and therapeutics through network-based approaches. Brief. Bioinform. *20*, 806–824. https://doi.org/10.1093/bib/bbx151.

16. Ryall, K.A., Holland, D.O., Delaney, K.A., Kraeutler, M.J., Parker, A.J., and Saucerman, J.J. (2012). Network reconstruction and systems analysis of cardiac myocyte hypertrophy signaling. J. Biol. Chem. *287*, 42259–42268. https://doi.org/10.1074/jbc.M112.382937.

17. Zeigler, A.C., Richardson, W.J., Holmes, J.W., and Saucerman, J.J. (2016). A computational model of cardiac fibroblast signaling predicts context-dependent drivers of myofibroblast differentiation. J. Mol. Cell. Cardiol. *94*, 72–81. https://doi.org/10.1016/j.yjmcc.2016.03.008.

18. Zeigler, A.C., Nelson, A.R., Chandrabhatla, A.S., Brazhkina, O., Holmes, J.W., and Saucerman, J.J. (2020). Computational model predicts paracrine and intracellular drivers of fibroblast phenotype after myocardial infarction. Matrix Biol. *91–92*, 136–151. https://doi.org/10.1016/j.matbio.2020.03.007.

19. Kuleshov, M.V., Jones, M.R., Rouillard, A.D., Fernandez, N.F., Duan, Q., Wang, Z., Koplev, S., Jenkins, S.L., Jagodnik, K.M., Lachmann,

A., et al. (2016). Enrichr: a comprehensive gene set enrichment analysis web server 2016 update. Nucleic Acids Res. *44*, W90–W97. https://doi.org/10.1093/nar/gkw377.

20. Hou, N., Wen, Y., Yuan, X., Xu, H., Wang, X., Li, F., and Ye, B. (2017). Activation of Yap1/Taz signaling in ischemic heart disease and dilated cardiomyopathy. Exp. Mol. Pathol. *103*, 267–275. https://doi.org/10.1016/j.yexmp.2017.11.006.

21. Lee, M.J., Byun, M.R., Furutani-Seiki, M., Hong, J.H., and Jung, H.S. (2014). YAP and TAZ regulate skin wound healing. J. Invest. Dermatol. *134*, 518–525. https://doi.org/10.1038/jid.2013.339.

22. Chothani, S., Schäfer, S., Adami, E., Viswanathan, S., Widjaja, A.A., Langley, S.R., Tan, J., Wang, M., Quaife, N.M., Jian Pua, C., et al. (2019). Widespread translational control of fibrosis in the human heart by RNA-binding proteins. Circulation *140*, 937–951. https://doi.org/10.1161/CIRCULATIONAHA.119.039596.

23. Ray, D., Yun, Y.C., Idris, M., Cheng, S., Boot, A., Iain, T.B.H., Rozen, S.G., Tan, P., and Epstein, D.M. (2020). A tumor-associated splice-isoform of MAP2K7 drives dedifferentiation in MBNL1-low cancers via JNK activation. Proc. Natl. Acad. Sci. USA *117*, 16391–16400. https://doi.org/10.1073/pnas.2002499117.

24. Cheng, A.W., Shi, J., Wong, P., Luo, K.L., Trepman, P., Wang, E.T., Choi, H., Burge, C.B., and Lodish, H.F. (2014). Muscleblind-like 1 (Mbnl1) regulates pre-mRNA alternative splicing during terminal erythropoiesis. Blood *124*, 598–610. https://doi.org/10.1182/blood-2013-12-542209.

25. Bugg, D., Bailey, L.R.J., Bretherton, R.C., Beach, K.E., Reichardt, I.M., Robeson, K.Z., Reese, A.C., Gunaje, J., Flint, G., DeForest, C.A., et al. (2022). MBNL1 drives dynamic transitions between fibroblasts and myofibroblasts in cardiac wound healing. Cell Stem Cell *29*, 419–433.e10. https://doi.org/10.1016/J.STEM.2022.01.012.

26. Khalil, H., Kanisicak, O., Prasad, V., Correll, R.N., Fu, X., Schips, T., Vagnozzi, R.J., Liu, R., Huynh, T., Lee, S.-J., et al. (2017). Fibroblast-specific TGF-β-Smad2/3 signaling underlies cardiac fibrosis. J. Clin. Invest. *127*, 3770–3783. https://doi.org/10.1172/JCI94753.

27. Del Re, D.P., Yang, Y., Nakano, N., Cho, J., Zhai, P., Yamamoto, T., Zhang, N., Yabuta, N., Nojima, H., Pan, D., and Sadoshima, J. (2013). Yes-associated protein isoform 1 (Yap1) promotes cardiomyocyte survival and growth to protect against myocardial ischemic injury. J. Biol. Chem. *288*, 3977–3988. https://doi.org/10.1074/jbc.M112.436311.

28. Molkentin, J.D., Bugg, D., Ghearing, N., Dorn, L.E., Kim, P., Sargent, M.A., Gunaje, J., Otsu, K., and Davis, J. (2017). Fibroblast-specific genetic manipulation of p38 mitogen-activated protein kinase in vivo reveals its central regulatory role in fibrosis. Circulation *136*, 549–561. https://doi.org/10.1161/CIRCULATIONAHA.116.026238.

29. Lacraz, G.P.A., Junker, J.P., Gladka, M.M., Molenaar, B., Scholman, K.T., Vigil-Garcia, M., Versteeg, D., de Ruiter, H., Vermunt, M.W., Creyghton, M.P., et al. (2017). Tomo-Seq identifies SOX9 as a key regulator of cardiac fibrosis during ischemic injury. Circulation *136*, 1396–1409. https://doi.org/10.1161/CIRCULATIONAHA.117.027832.

30. Furumatsu, T., Tsuda, M., Taniguchi, N., Tajima, Y., and Asahara, H. (2005). Smad3 induces chondrogenesis through the activation of SOX9 via CREB-binding protein/p300 recruitment. J. Biol. Chem. *280*, 8343–8350. https://doi.org/10.1074/jbc.M413913200.

31. Yasuda, H., Oh, C.d., Chen, D., De Crombrugghe, B., and Kim, J.H. (2017). A novel regulatory mechanism of type II collagen expression via a SOX9-dependent enhancer in intron 6. J. Biol. Chem. *292*, 528–538. https://doi.org/10.1074/jbc.M116.758425.

32. Bugg, D., Bretherton, R., Kim, P., Olszewski, E., Nagle, A., Schumacher, A.E., Chu, N., Gunaje, J., DeForest, C.A., Stevens, K., et al. (2020). Infarct collagen topography regulates fibroblast fate via p38-yap-TEAD signals. Circ. Res. *127*, 1306–1322. https://doi.org/10.1161/CIRCRESAHA.119.316162.

33. Cui, S., Liu, Z., Tao, B., Fan, S., Pu, Y., Meng, X., Li, D., Xia, H., and Xu, L. (2021). miR-145 attenuates cardiac fibrosis through the AKT/GSK-3β/β-catenin signaling pathway by directly targeting SOX9 in fibroblasts. J. Cell. Biochem. *122*, 209–221. https://doi.org/10.1002/jcb.29843.

34. Chen, W., Ma, J., Zhu, G., Jules, J., Wu, M., McConnell, M., Tian, F., Paulson, C., Zhou, X., Wang, L., and Li, Y.P. (2014). Cbfβ deletion in mice recapitulates cleidocranial dysplasia and reveals multiple functions of Cbfβ required for skeletal development. Proc. Natl. Acad. Sci. USA *111*, 8482–8487. https://doi.org/10.1073/pnas.1310617111.

35. Islam, M.N., Itoh, S., Yanagita, T., Sumiyoshi, K., Hayano, S., Kuremoto, K.-I., Kurosaka, H., Honjo, T., Kawanabe, N., Kamioka, H., et al. (2015). Runx/Cbfb signaling regulates postnatal development of granular convoluted tubule in the mouse submandibular gland. Dev. Dyn. *244*, 488–496. https://doi.org/10.1002/dvdy.24231.

36. Komori, T. (2015). The functions of Runx family transcription factors and Cbfb in skeletal development. Oral Sci. Int. *12*, 1–4. https://doi.org/10.1016/S1348-8643(14)00032-9.

37. Brown, D.I., Cooley, B.C., Quintana, M.T., Lander, C., and Willis, M.S. (2016). Nebulized delivery of the MAPKAP kinase 2 peptide inhibitor MMI-0100 protects against ischemia-induced systolic dysfunction. Int. J. Pept. Res. Ther. *22*, 317–324. https://doi.org/10.1007/s10989-015-9507-3.

38. Mia, M.M., Cibi, D.M., Ghani, S.A.B.A., Singh, A., Tee, N., Sivakumar, V., Bogireddi, H., Cook, S.A., Mao, J., Singh, M.K., et al. (2022). Loss of Yap/Taz in cardiac fibroblasts attenuates adverse remodelling and improves cardiac function. Cardiovasc. Res. *118*, 1785–1804. https://doi.org/10.1093/CVR/CVAB205.

39. Singer, J.W., Fleischman, A., Al-Fayoumi, S., Mascarenhas, J.O., Yu, Q., and Agarwal, A. (2018). Inhibition of interleukin-1 receptor-associated kinase 1 (IRAK1) as a therapeutic strategy. Oncotarget *9*, 33416–33439. https://doi.org/10.18632/oncotarget.26058.

40. Bageghni, S.A., Hemmings, K.E., Yuldasheva, N.Y., Maqbool, A., Gamboa-Esteves, F.O., Humphreys, N.E., Jackson, M.S., Denton, C.P., Francis, S., Porter, K.E., et al. (2019). Fibroblast-specific deletion of IL-1 receptor-1 reduces adverse cardiac remodeling following myocardial infarction. JCI Insight *5*, e125074. https://doi.org/10.1172/jci.insight.125074.

41. Gorelik, M., Lee, Y., Abe, M., Andrews, T., Davis, L., Patterson, J., Chen, S., Crother, T.R., Aune, G.J., Noval Rivas, M., and Arditi, M. (2019). IL-1 receptor antagonist, anakinra, prevents myocardial dysfunction in a mouse model of Kawasaki disease vasculitis and myocarditis. Clin. Exp. Immunol. *198*, 101–110. https://doi.org/10.1111/cei.13314.

42. Zhao, S., Kurenbekova, L., Gao, Y., Roos, A., Creighton, C.J., Rao, P., Hicks, J., Man, T.K., Lau, C., Brown, A.M.C., et al. (2015). NKD2, a negative regulator of Wnt signaling, suppresses tumor growth and metastasis in osteosarcoma. Oncogene *34*, 5069–5079. https://doi.org/10.1038/onc.2014.429.

43. Tao, H., Yang, J.J., Shi, K.H., and Li, J. (2016). Wnt signaling pathway in cardiac fibrosis: new insights and directions. Metabolism *65*, 30–40. https://doi.org/10.1016/j.metabol.2015.10.013.

44. Huebener, P., Abou-Khamis, T., Zymek, P., Bujak, M., Ying, X., Chatila, K., Haudek, S., Thakker, G., and Frangogiannis, N.G. (2008). CD44 is critically involved in infarct healing by regulating the inflammatory and fibrotic response. J. Immunol. *180*, 2625–2633. https://doi.org/10.4049/jimmunol.180.4.2625.

45. Yang, L.-W., Qin, D.-Z., James, E., McKallip, R.J., Wang, N.-P., Zhang, W.-W., Zheng, R.-H., Han, Q.-H., and Zhao, Z.-Q. (2019). CD44 deficiency in mice protects the heart against angiotensin ii-induced cardiac fibrosis. Shock *51*, 372–380. https://doi.org/10.1097/SHK.0000000000001132.

46. Pang, X.F., Lin, X., Du, J.J., and Zeng, D.Y. (2020). LTBP2 knockdown by siRNA reverses myocardial oxidative stress injury, fibrosis and remodelling during dilated cardiomyopathy. Acta Physiol. *228*, e13377. https://doi.org/10.1111/apha.13377.

47. Parichatikanond, W., Luangmonkong, T., Mangmool, S., and Kurose, H. (2020). Therapeutic targets for the treatment of cardiac fibrosis and cancer: focusing on tgf-β Signaling. Front. Cardiovasc. Med. *7*, 34. https://doi.org/10.3389/fcvm.2020.00034.

48. Niu, Z., Conway, S.J., Martin, J.F., Ivey, K., Srivastava, D., Nordheim, A., and Schwartz, R.J. (2008). Serum response factor orchestrates nascent sarcomerogenesis and

silences the biomineralization gene program in the heart. Proc. Natl. Acad. Sci. USA *105*, 17824–17829. https://doi.org/10.1073/pnas.0805491105.

49. Trembley, M.A., Quijada, P., Agullo-Pascual, E., Tylock, K.M., Colpan, M., Dirkx, R.A., Myers, J.R., Mickelsen, D.M., De Mesy Bentley, K., Rothenberg, E., et al. (2018). Mechanosensitive gene regulation by myocardin-related transcription factors is required for cardiomyocyte integrity in load-induced ventricular hypertrophy. Circulation *138*, 1864–1878. https://doi.org/10.1161/CIRCULATIONAHA.117.031788.

50. Li, M., Wu, J., Hu, G., Song, Y., Shen, J., Xin, J., Li, Z., Liu, W., Dong, E., Xu, M., et al. (2021). Pathological matrix stiffness promotes cardiac fibroblast differentiation through the POU2F1 signaling pathway. Sci. China Life Sci. *64*, 242–254. https://doi.org/10.1007/s11427-019-1747-y.

51. Landry, N.M., Rattan, S.G., and Dixon, I.M.C. (2019). An improved method of maintaining primary murine cardiac fibroblasts in two-dimensional cell culture. Sci. Rep. *9*. https://doi.org/10.1038/s41598-019-49285-9.

52. Herum, K.M., Choppe, J., Kumar, A., Engler, A.J., and McCulloch, A.D. (2017). Mechanical regulation of cardiac fibroblast profibrotic phenotypes. Mol. Biol. Cell *28*, 1871–1882. https://doi.org/10.1091/mbc.E17-01-0014.

53. Tan, P.M., Buchholz, K.S., Omens, J.H., McCulloch, A.D., and Saucerman, J.J. (2017). Predictive model identifies key network regulators of cardiomyocyte mechano-signaling. PLoS Comput. Biol. *13*, e1005854. https://doi.org/10.1371/journal.pcbi.1005854.

54. Schindelin, J., Arganda-Carreras, I., Frise, E., Kaynig, V., Longair, M., Pietzsch, T., Preibisch, S., Rueden, C., Saalfeld, S., Schmid, B., et al. (2012). Fiji: an open-source platform for biological-image analysis. Nat. Methods *9*, 676–682. https://doi.org/10.1038/nmeth.2019.

55. GitHub. (2015). - saucermanlab/Netflux: Netflux is a user-friendly software for developing dynamic computational models of biological networks. Models are created in Excel format and then simulated using the Netflux graphical interface. No computer programming is required. Netflux is written in MATLAB, with binary versions available for Windows and. MacOS. https://github.com/saucermanlab/Netflux.

56. Kraeutler, M.J., Soltis, A.R., and Saucerman, J.J. (2010). Modeling cardiac β-adrenergic signaling with normalized-Hill differential equations: comparison with a biochemical model. BMC Syst. Biol. *4*, 157. https://doi.org/10.1186/1752-0509-4-157.

57. Landry, N.M., Rattan, S.G., and Dixon, I.M.C. (2019). An improved method of maintaining primary murine cardiac fibroblasts in two-dimensional cell culture. Sci. Rep. *9*, 12889. https://doi.org/10.1038/s41598-019-49285-9.

58. Stempien-Otero, A., Kim, D.-H., and Davis, J. (2016). Molecular networks underlying myofibroblast fate and fibrosis. J. Mol. Cell. Cardiol. *97*, 153–161. https://doi.org/10.1016/j.yjmcc.2016.05.002.

STAR★METHODS

KEY RESOURCES TABLE

REAGENT or RESOURCE	SOURCE	IDENTIFIER
Antibodies		
Anti-αSMA	Sigma-Aldrich	Cat# A2547, RRID:AB_476701
Anti-GAPDH	Fitzgerald Industries International	Cat# 10R-2932, RRID:AB_11199818
Anti-Muscleblind-like 1 [MBNL1]	Abcam	Abcam Cat# ab45899, RRID:AB_1310475
Anti- Osteoblast specific factor 2 [Postn]	BioVendor	RRID:AB_344577
Anti- p38 MAP Kinase	Cell Signaling	9212L
Anti-phospho p38 Map Kinase	Cell Signaling	9211L
Goat AntiRabbit IgGHRP	Millipore Sigma	AP307P
Bacterial and virus strains		
AdCre	Davis et. Al[1]	N/A
AdβGal	Davis et. Al[5]	N/A
Chemicals, peptides, and recombinant proteins		
CollagenaseType 2	Worthington	Cat #: LS004176
DMEM High Glucose	Fisher Scientific	Cat #: 10-017-CV
Liberase TH	Sigma Aldrich	Cat #: 5401151001
Characterized FBS	Fisher Scientific	Cat #: SH3007103
Penicillin-Streptomycin	Fisher Scientific	Cat #: 15140122
1M Tris-HCl pH 7.4	ThermoFisher	Cat #: 15567027
5M NaCl	ThermoFisher	Cat #: AM9760G
PVDF Membrane	Bio-Rad	Cat #: 1620177
SDS	Sigma Aldrich	Cat #: L4509
Coomassie	Diversified Biotech	Cat #: RCS-50
30% Acrylamid/Bis	Bio-Rad	Cat #: 1610156
Critical commercial assays		
Supersignal west pico plus chemilumenescent substrate	Thermo Fisher	Cat #: 34580
Deposited data		
Rat Cardiac Fibroblasts RIP-seq	Davis et. Al[1]	GEO: GSE74185
Mouse Embryonic Fibroblast RNAseq	Davis et. Al[1]	GEO: GSE74185
Experimental models: Cell lines		
MBNL1$^{Fl/Fl}$Cardiac Fibroblasts	Primary isolation	N/A
Experimental models: Organisms/strains		
B6;B6N-Mbnl1tm1a(EUCOMM)Wtsi	Bugg et. Al[25]	N/A
Software and algorithms		
Matlab Software	MathWorks	https://www.mathworks.com/products/matlab.html
MBNL1 Fibroblast Network Model and Code	This paper	https://doi.org/10.5281/zenodo.7641538
Python version 3.8	Python Software Foundation	https://www.python.org
Netflux Modeling Software	Saucerman Lab, University of Virginia	https://github.com/saucermanlab/Netflux
Biorender (for graphical abstract)	Biorender	https://biorender.com/
imageJ	Schindelin et al.[54]	https://imagej.net/software/fiji/
GraphPad Prism (v9.0)	GraphPad Software	https://www.graphpad.com:443/ RRID:SCR_002798

RESOURCE AVAILABILITY

Lead contact

Further information and requests for resources and reagents should be directed to and will be fulfilled by the lead contact, Dr. Jeffrey Saucerman (jsaucerman@virginia.edu).

Materials availability

Reagents used in this study that are not commercially available or obtainable through repositories will be shared upon reasonable request and completion of a material transfer agreement (MTA).

Data and code availability

- All original code has been deposited at Zenodo and Github and is publicly available as of the date of publication. The DOI is listed in the key resources table.
- RNAseq and RIPseq data used in this study, originally from our previous study,[1] are deposited at GEO and are publicly available as of the date of publication. Accession numbers are listed in the key resources table.
- Any additional information required to reanalyze the data reported in this paper is available from the lead contact upon request.

EXPERIMENTAL MODEL AND SUBJECT DETAILS

All animal experimentation was approved by the University of Washington's Institutional Animal Care and Use Committee. As previously described[25] MBNL1 knockout mice ($MBNL1^{Fl/Fl}$) were generated using targeted C57BL/6 embryonic stem cells (ES) from the International Knockout Mouse Consortium (IKMC). Founders were bred onto a C57BL/6 background and then to mice expressing Flippase to excise the LacZ-neomycin cassettes still present within the floxed MBNL1 allele, as IKMC uses a knockout first approach for their targeted alleles. Once the LacZ-neomycin cassettes were flipped-out, $MBNL1^{Fl/Fl}$ mice were bred to homozygosity.

METHOD DETAILS

Analysis of a genome-wide cDNA αSMA reporter luciferase screens

Our genome-wide gain-of-function screen was performed in our previous study.[1] The objective of the cDNA screen was to identify drivers of *Acta2* promoter activity. In that study, quiescent mouse embryonic fibroblasts were transfected with one of 18,400 cDNAs and an *Acta2* (αSMA) promoter reporter construct, on 384-well plates. Here, raw assay value Excel files were processed in Python version 3.8. Raw values were normalized so that plate median values across all 45 plates were equal. We used the following equation to calculate normalized screen values: $NormalizedValue = OriginalValue * \left(\frac{ScreenWideMedian}{PlateMedian}\right)$. Hits were determined by z-score relative to other reads from the same plate. The normalized screen values with plate-based z-scores in the top 5% were considered hits. Hits were reasonably evenly distributed across the screen plates.

Data overlap and putative MBNL1 target prioritization

We overlapped four omics datasets involving perturbed MBNL1 signaling or *Acta2* promoter activity to identify putative fibrotic regulators downstream of MBNL1. The omics data used for this study are as follows: 1) A genome-wide cDNA αSMA reporter luciferase screen described above.[1] 2) Mouse embryonic fibroblast (MEF) RNAseq: treatment groups include WT, WT+TGFβ, MBNL1 overexpression (MBNL1-OE), MBNL1 knockout (MBNL1-KO), and MBNL1-KO+TGFβ.[1] 3) RNAseq data in mouse cardiac fibroblasts isolated after myocardial infarction: treatments include WT and MBNL1-OE. Fibroblasts were isolated following MI.[25] 4) Rat cardiac fibroblast (RCF) RNA Immunoprecipitation Sequencing (RIPseq): treatment groups include WT and MBNL1-OE. For this study, we used a published table of RIPseq results for genes bound, alternatively spliced, or alternatively polyadenylated by MBNL1.[1] The MEF RNAseq and RCF RIPseq data used in this study were processed and published in our previous study.[1] We determined two priority levels for these data overlaps.

First priority overlaps

We identified two categories of genes as our first priority overlaps

First, we identified genes bound by MBNL1 in RCF RIPseq that were also a hit in the *Acta2* promoter luciferase reporter cDNA screen. These genes are likely directly regulated by MBNL1, and likely signal through

pathways that regulate α-Smooth Muscle Actin (α-SMA) expression, a canonical marker of fibroblast activation.

Second, we looked at genes with differential expression (DE) in MBNL1-OE versus WT in *in vivo* RNAseq in MCFs that were bound by MBNL1 in the RIPseq. These genes are bound by MBNL1 and show increased mRNA expression upon*in vivo* MBNL1-OE in cardiac fibroblasts.

Genes derived from first-priority overlaps were considered candidate regulators during model expansion.

Second priority overlaps

We designated second priority targets as mRNAs bound by MBNL1 in RCF RIPseq that had an mRNA expression fold change of >=1.5 upon various MBNL1 perturbations in MEF RNAseq (Figures S1C–S1E). These gene sets were deemed second priority because the MEF RNAseq data is not cardiac specific and does not confirm that a candidate gene can influence αSMA expression.

Genes from second-priority overlaps were used primarily to reinforce confidence in genes from the first-priority list.

Fibroblast network model expansion with MBNL1

Literature search to evaluate a role in fibrosis for candidate regulators was performed by entering 'gene name + cardiac fibrosis' in PubMed. The fibroblast signaling network model was expanded from the most recently published version[18] to incorporate MBNL1 and its putative targets. Models were generated for use in MATLAB with Netflux software[55] using a logic-based differential equation approach.[56] Signaling relationships between nodes were supported by at least two independent sources in fibroblasts, or fibroblast-similar cell types, prioritizing cardiac fibroblasts. Baseline node input weights were set to 0.1, except for *inputMechanical*which was set to 0.725 to represent the mechanical load imposed by conventional tissue culture plates, as the model is built upon*in vitro* studies of cultured cells.[57] *EC50* and *n* parameters were set to 0.6 and 1.4 respectively per the previously published model. MBNL1-target reactions were connected using AND gates with other inputs to the target node with a weight of 1.0 (e.g. 'Akt & MBNL1 => LOX'). Input reactions to MBNL1 targets have separate OR gate reactions with a weight of 0.5 (e.g. 'Akt => LOX'), to represent a weak activation in the absence of MBNL1 (Figure 2A). The reaction weight for Runx and Cbfβ activation of smad3 was set to 0.6, as this improved AND-gated smad3 activation in low MBNL1 signaling contexts compared to 0.5. This approach was designed to recapitulate results from our previous study, where targets showed partial activation in MBNL1 absent conditions, decreased from WT, and increased activation upon MBNL1-OE transfection.[58] Input reactions were included for select nodes with basal activation currently unexplained by the model (w = 0.25 for Sox9 and Foxo3; w = 0.5 for SRFmRNA and Cbfβ). TGFβ mRNA feedback reactions have weights of 0.6 per the previously published model version.[1] All other reaction weights are 1.0.

Model simulations

Ensemble simulations

We employed a method for ensemble simulation modified from a previous study to evaluate the robustness of model predictions.[18] Weights for input reactions for basal values were randomly sampled from normal distributions with respective means of 0.1 for basal inputs, 0.725 for mechanical stretch, and 0.6 for high inputs. To determine the coefficient of variation (COV) for input reaction weights, ensemble simulations measuring αSMA output COV in response to high TGFβ were run for N = 1000, iterating input COVs from 0.030 to 0.36 by 0.01 each iteration. The MATLAB polyfit function was used to fit a line and determine that an input reaction weight COV of 0.0331 resulted in the experimentally determined αSMA output COV of 0.2606.[1] The COV was multiplied by the weight mean to determine standard deviation for normal-random sampling. Randomly sampled values that fell outside of the 0–1 range were resampled until the sampled value was within range. Simulations were run 150 times. The N of 150 for the ensemble simulations was determined by running model simulations with normal randomly sampled input values and measuring the change in average validation percentage for intermediate-ouput validation with each additional simulation. N was determined when the average change of mean validation for the most recent five simulations was <0.005 (Figure S2). Modeling was performed using MATLAB version 2021b and the MATLAB Statistics and Machine Learning toolbox for random sampling.

Model validation

Model validation relationships were divided into two categories: 'Input-Output' and 'Intermediate-Output'. 'Input-Output' relationships were determined as previously described, and the validation set from the original published model was used.[17] As the 'Intermediate-Output' validations recapitulate specific experiments for more novel fibrosis regulators, one publication was used for each relationship. Sources were found by searching for 'target name' and 'fibrosis' in PubMed. Experiments in cardiac fibroblasts, or similar cell types, were prioritized in cases of conflicting evidence. Overexpression experiments were represented by changing y0 of the node to 1, with tau set to 10000 to prevent significant change during the simulation. Inhibition studies were represented by reducing y0 of the node to 0. Weight means for elevated input simulations were set to 0.75, 25% above the default EC50 value, except mechanical stimulus which was set to 1.0. Input values were randomly sampled around respective means as described above. A threshold of 0.001 was used to determine if simulated experiments predicted an 'increase', 'decrease', or 'no change'.

Perturbation screens for MBNL1 target influence on αSMA expression

A baseline simulation of the network model was used to obtain control node values at steady state (t = 500). For the knockdown screen, AngII and TGFβ input reaction weight means were set to 0.6, as these ligands activate MBNL1 and MBNL1 target expression.[1] Under the high AngII+TGFβ simulation conditions, the ymax of each putative MBNL1 target node and MBNL1 were sequentially set to 0 to represent knockdown. For the overexpression screen, the y0 of sequential nodes was set to 1, with tau set to 10000. For overexpression simulations in Figures 4 and 5, AngII and TGFβ input means were raised from 0.1 to 0.25 to increase network-wide signaling without saturating profibrotic signaling.

Overexpression simulations to investigate MBNL1 target signaling mechanisms

A baseline simulation of the network model was used to obtain control node values at steady state (t = 500). For MBNL1 overexpression simulations, MBNL1 y0 was set to 1 with tau set to 10000. MBNL1 targets were overexpressed as described above and change in network node activity compared to the baseline simulation was measured.

In vitro experiments

Mouse primary cardiac fibroblast isolation

Cardiac fibroblasts were isolated by retrograde Langendorff perfusion with type II collagenase (2mg/ml) and liberase blendzyme (0.4mg/ml) solubilized in Krebs-Henseleit buffer as previously described.[28,32] Fibroblasts were pelleted after digestion and resuspended in Dulbecco's Minimal Essential Media (DMEM) with high glucose and supplemented with 1% penicillin and streptomycin (P/S), and 20% fetal bovine serum (FBS). MBNL1 floxed cardiac fibroblasts were treated with either Adenoviral Cre (MOI 500) or Adenoviral βGal (MOI 500) overnight in 2% serum media at passage 1 to permanently excise MBNL1. Adenoviral βGal was used as a viral control. Fibroblasts were further expanded for an additional passage before collecting in cold RIPA lysis buffer [5 M NaCl, 10% Triton-X 100, 25%SDS, 1 M Tris-Cl PH 7.4] and storing at −80°C.

Western blot

RIPA Lysates were diluted in Laemmli buffer, 5–60 μg of protein was loaded into a 10% SDS-PAGE acrylamide gels and transferred to PVDF membrane for immunodetection. Total p38 was detected with anti-p38 (1:1000, rabbit polyclonal antibody, Cell Signaling 60 μg protein) overnight at 4°C with goat anti-rabbit HRP conjugate secondary at 1:10,000 from Santa Cruz Biotechnology for 1 hour. Phosphorylated p38 was detected with anti-Pp38 (1:1000, rabbit polyclonal antibody, Cell Signaling 60 μg protein) overnight at 4°C with goat anti-rabbit HRP conjugate secondary at 1:10,000 from Santa Cruz Biotechnology for 1 hour. MBNL1 was detected with anti-MBNL1 (1:500, mouse monoclonal antibody, Abcam 60 μg protein) overnight at 4°C with goat anti-mouse HRP conjugate secondary at 1:10,000 from Santa Cruz Biotechnology for 1 hour. αSMA was detected with anti-actin alpha SMA (1:1000, mouse monoclonal antibody, Sigma 5 μg protein) overnight at 4°C with goat anti-mouse HRP conjugate secondary at 1:10,000 from Santa Cruz Biotechnology for 1 hour. Periostin was detected with anti-Osteoblast specific factor 2 (1:200, rabbit polyclonal antibody, BioVendor 5μg protein) overnight at 4°C with goat anti-rabbit HRP conjugate secondary at 1:10,000 from Millipore Sigma for 1 hour. Blots were visualized using SuperSignal West Pico Plus Chemiluminescent Substrate on a Biorad ChemiDoc. As p38 and phospho-p38 have similar molecular

weights to GAPDH, westerns for each protein were run on individual gels and visualized on individual membranes. The GAPDH membrane was also Coomassie stained to ensure equal protein loading on the gel (Figure S6). Each membrane was loaded with 4 samples for both the WT group and the MBNL1-KO group.

QUANTIFICATION AND STATISTICAL ANALYSIS

Computational model simulations were performed using MATLAB 2022b and the 'Statistics and Machine Learning Toolbox'. Quantification of Western blotdata was performed using ImageJ[54] software and statistical analysis was performed using GraphPad Prism version 9.0. Error bars for all figures represent standard error of the mean (S.E.M.) across all samples for experimental data, and all simulations in the ensemble for computational model data.